Design and Optimization of a Planar Biped Leg Based on Direct Drive Linear Actuators

M. Langard, Ph. Lucidarme, N. Delanoue, R. Guyonneau, Franck Mercier, C. Chevallereau, Ph. Wenger, Y. Aoustin

Hindawi
Mathematical Problems in Engineering
Volume 2022, Article ID 6455182, 15 pages
https://doi.org/10.1155/2022/6455182

Research Article

Design and Optimization of a Planar Biped Leg Based on Direct Drive Linear Actuators

M. Langard,[1] **Ph. Lucidarme**,[1] **N. Delanoue**,[1] **R. Guyonneau**,[1] **F. Mercier**,[1] **C. Chevallereau**,[2] **Ph. Wenger**,[2] **and Y. Aoustin**[2]

[1]*Laboratoire Angevin de Recherche en Ingénierie des Systèmes (LARIS), 49000 Angers, France*
[2]*Laboratoire des Sciences Du Numérique de Nantes (LS2N), UMR CNRS 6004, 44321 Nantes, France*

Correspondence should be addressed to M. Langard; morgan.langard@outlook.fr

Received 9 March 2022; Accepted 17 May 2022; Published 28 June 2022

Academic Editor: Carlos Llopis-Albert

The choice of actuation when designing a bipedal robot is an important matter, as it impacts its capacities and its control. In these aspects, electric direct-drive (DD) linear motors are interesting candidates. Indeed, they can reproduce the human muscle system by using monoarticular and bi-articular motors and offer a natural backdrivability for impact mitigation. However, motor efficiency depends on their elongation and their attachment points. The ROBIBIO (RObot humanoïde BI-articulaire BIO-inspiré) project aims to design and build a planar bipedal robot using electric direct-drive linear motors for the actuation. To do so, a simulator was developed to evaluate multiple human-like bipedal robot architectures over a set of motion-captured movements. Furthermore, a numerical optimization was done to find the best motor placement for each architecture.

1. Introduction

One shortcoming of generic robots is their capability of evolving in their environment, which results in either tracked or wheeled mechanisms. However, it limits their use to nearly 50% of Earth's landmass, which is unsuitable for such movement schemes [1]. This limitation motivates the design of bipedal walking robots as the human locomotion system allows one to perform a wide range of motions in uneven environments. However, biped motions such as squatting, walking, or running are complex to perform. They require the actuation system to produce forces with important variations and to be able to cope with impacts on the ground. Moreover, the forces required from the motors will be greatly influenced by the robot's parameters. Therefore, choosing a relevant leg architecture and motors for the actuation is of utmost importance when designing a bipedal robot. Concerning the motor type, there are two main solutions: rotary and linear motors. To take into account the impacts involved in classic biped motions, one can consider the use of backdrivable motors as they offer inherent low-impedance and impact mitigation [2–8].

Rotary motors are a popular option for current bipedal robots. Their characteristics are well known from being used for multiple decades in industrial robots such as the PUMA in the 80s and later on for humanoid robots like the Honda [9]. This type of motor allows unlimited joint rotation and can be connected to a reduction gear to increase the output torque. Such motors have some drawbacks. The output axis must be aligned with the articulated bodies to avoid dynamic imbalance. They also have limited backdrivability whenever a reduction gear is used. Research was done to cope with the low backdrivability by using a variable stiffness mechanism [4] or selective elastic actuators [10]. The latter adds control complexity and limitations to the actuation bandwidth. An alternative is the use of Direct-Drive (DD) actuators, but DD rotative motors have limited torque and might require the addition of a low-ratio gearbox. This forces one to compromise between motor size, backdrivability, bandwidth, and output torque [8, 11].

Linear motors can also be considered (see Figure 1). They allow for more freedom when designing a leg architecture, and a lot of systems are naturally backdrivable. Some examples are pneumatic and hydraulic motors [5, 6]. Unfortunately, compressors are an issue for embedded systems and hydraulic motors are costly, heavy, and noisy. We believe DD electric motors have better potential in these aspects as they have good dynamic properties, allowing direct control over the output force [12]. Such motors, having high backdrivability, can produce high forces at high speeds. They also mimic the human muscular system, making them good candidates to design a human-like bipedal robot.

Another aspect is the use of motors in bi-articular position. A motor in bi-articular position actuates two consecutive joints. This is contrary to a monoarticular one, which affects only one joint. Doorenbosch et al. [13] showed that mono and bi-articular muscles are present in the human leg structure, making such motors an option to consider. A design methodology for bipedal robots using a combination of monoarticular and bi-articular DD linear motors is proposed in [3], as well as some architectures without redundancy selected to perform a computed trajectory. As most bipedal robots limit themselves to nonredundant architectures, redundancy while using linear actuators is still a subject to be explored.

This paper proposes to go further by studying different architectures involving monoarticular and bi-articular DD linear motors with and without redundancy, as well as evaluating their efficiency when performing a movement to ultimately build a bipedal robot using such motors. Another originality in our approach is to base our work on motion-captured motions in order to reinforce the biomimetic aspect of the robot. To do so, a simulator was built to evaluate potential designs. A numerical optimization was also implemented to obtain optimal placement of the motors for each architecture, as shown in Figure 2.

This paper will be organized as follows: first, the problem and methodology will be presented. We will then explain the simulator's behavior before presenting the obtained results and discussing them.

2. Problem Statement

2.1. Selected Architectures and Geometries. Even though it was decided to use linear motors, their number as well as their placement on a robotic leg still needs to be fixed. The rotation of the joint using linear motors is done through the elongation of the actuator. In this aspect, some of the followed guidelines are as follows:

(i) The motor's positions should be similar to their equivalent muscles in the human body when possible.

(ii) Each motor should be unique in the considered architecture to keep the design simple

(iii) Even when considering redundancy, the number of motors should still be limited to conserve the human-like aspect and reduce its weight

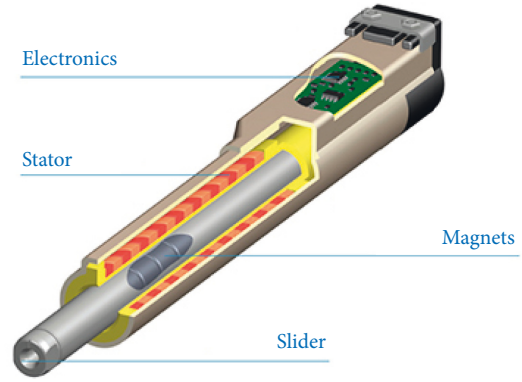

Figure 1: An example of a DD electric linear actuator.

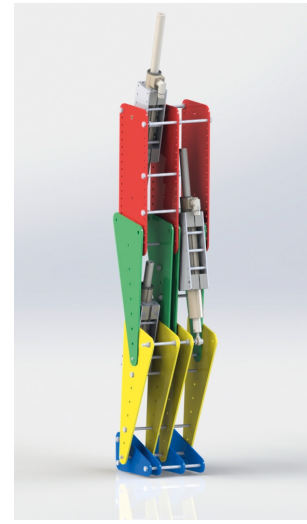

Figure 2: Computer-aided design of the obtained optimal monoarticular architecture.

This resulted in considering a monoarticular motor for each joint (hip, knee, and ankle) and two bi-articular actuators spanning the hip-knee joints and knee-ankle joints, respectively, for a maximum of five motors. From these choices, 14 architectures, i.e., motor's type and number, are deduced, taking as a base the nonredundant architectures presented in [3], and adding six architectures with redundancy (5 four-motor architectures and one five-motor architecture, shown in Figure 3). The motors used in each architecture are detailed in Figure 4.

Once the studied architectures are decided, what remains is the choice of the position of the fixation points on the robot limbs for all the motors. This is what we call the geometry of a robot. Per the previous guidelines, the geometry should conserve the human-like aspect of the biped while ensuring its capacity to perform a given motion. Indeed, as long as linear motors are used, a singularity will occur whenever the motor's axis intersects with the joint axis. In this singular configuration, no force can be transmitted to the joint. This states a problem where the motor's position must avoid singularities during the motion but should still be close enough to the limbs as to keep the robot

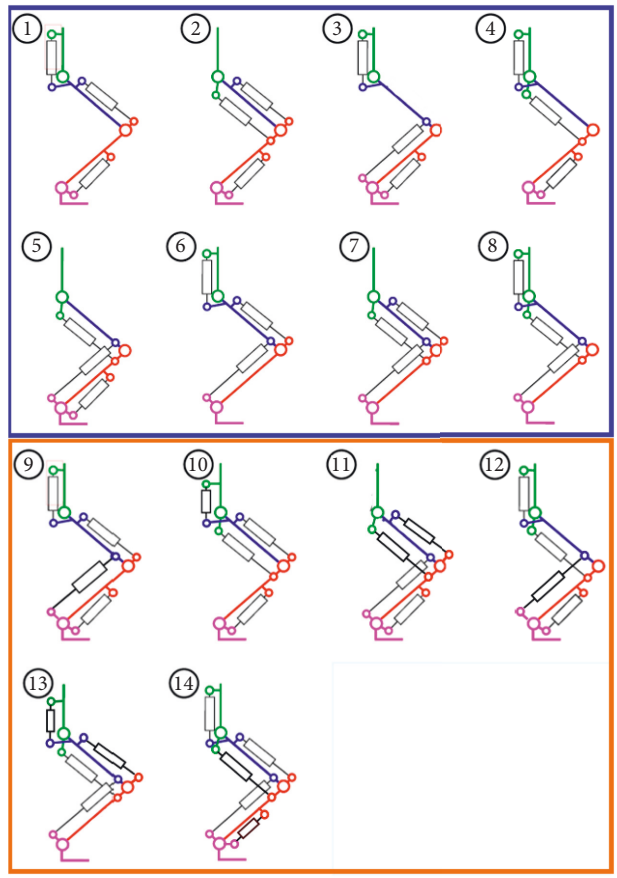

Figure 3: Architectures (blue: nonredundant/orange: redundant).

	Hip	Knee	Ankle	Hip-knee	Knee-ankle	Architecture
3 motors	■	■	■			1
		■	■	■		2
	■		■		■	3
	■		■	■		4
			■	■	■	5
	■	■			■	6
		■		■	■	7
	■			■	■	8
4 motors	■	■	■		■	9
	■	■	■	■		10
		■	■	■	■	11
	■		■	■	■	12
	■	■		■	■	13
5 motors	■	■	■	■	■	14

Figure 4: Motors used for each architecture.

size within human-like proportions. The latter leads to defining a bounded area around each limb where the motor attachments should be placed.

2.2. Direct Drive (DD) Electric Linear Motor. DD-electric linear motors have a structure similar to rotative ones. Both have a static stator, but while a rotative motor has a movable rotor to generate rotation, a linear motor has a slider to produce translation. The stator is composed of multiple coils that will create an electromagnetic field when circulating an electric current. This will in turn fix the position of the slider. An interesting feature of this mechanism is that it allows one to tune the resistance to perturbations with the input current. This creates a virtual spring to absorb shocks. The geometry required for such a robot comes directly from the use of linear motors.

With a linear motor, the torque is not generated directly like a rotative one but comes from the available leverage between the motor axis and the affected joint axis. A singularity problem can occur and must be taken into account. Moreover, the maximal available force of a linear motor is dependent on its elongation, as seen in Figure 5, which reinforces the importance of geometry.

2.3. Formal Problem Statement. Our goal is to find the best architecture among the candidates along with its optimal geometry in order to perform a given motion. As the motor singularities and torques required from them depend on the configuration of the biped, the results will depend on the studied motions. A set of motions comprised squats, walking, and running at different speeds can be selected to have multiple kinds of motions at different intensities. A simulator was implemented in order to evaluate the performance of an architecture A (with $A \in \{1, \ldots, 14\}$, see Figure 3) and one of its geometries P (see Figure 6). In other words, for a fixed architecture, multiple geometries are evaluated to obtain the best suited for the chosen motions.

The evaluated criterion is the feasibility $M_A(P)$ of the motion using the geometry P, defined as

$$M_A(P) = \frac{1}{T}\int_0^T b_A(P,t)\mathrm{d}t, \tag{1}$$

where $[0, T]$ is the time interval of interest. We define the Boolean $b_A(P,t)$ as true if and only if all the required forces to actuate the joints can be produced by the linear motors of the given architecture A. The criterion of feasibility represents the doable percentage for the considered motion with the given architecture and the given geometry.

3. Simulator

3.1. Workflow. The simulator's behavior is shown on Figure 7, with the input being the following:

$(\overline{x}_i, \overline{y}_i) \in [a_i, b_i] \times [c_i, d_i]$ the higher 2D anchor point, $(\underline{x}_i, \underline{y}_i)$ the lower 2D anchor point, and $o_i \in [e_i, f_i]$ the offset of each motor. For each motor, the five-dimensional vector $p_i = (\overline{x}_i, \overline{y}_i, \underline{x}_i, \underline{y}_i, o_i)$ combines the 2D positions of its anchor points and the offset. This brings either 15, 20, or 25 optimization variables depending on the considered architecture. For instance, with architecture 1, the geometry P is of the following form: (p_1, p_2, p_3).

$q(t)$ the joint configuration at time t of the studied motion, obtained from the HuMoD database [14].

$\Gamma(t)$ the joint torques at time t of the studied motion, computed from $t \mapsto q(t)$ with the Newton–Euler formalism.

It is relevant to remark that even though $q(t)$ and $\Gamma(t)$ are coherent between one another. But in reality, the latter is dependent on P. In our approach, we assume that the position of the linear motors should not affect neither the mass repartition nor the inertia matrices of the different limbs.

The Boolean $b_A(P,t)$ is computed by comparing at each instant t, the forces $F(t)$ required from the motors with the maximum forces available from them $\overline{F}(P, q(t))$; formally,

$$b_A(P,t) \Leftrightarrow F(t) \leq \overline{F}(P, q(t)). \tag{2}$$

The latter is then integrated over time and outputs the feasibility denoted by $M_A(P)$.

3.2. Forces Computation. As a linear motor cannot produce directly a torque but instead generate a force along the motor's axis, some transformation is needed to convert this forces into a torque. The relationship between the two also depends on the number and positioning (i.e., the affected joints) of the motors. As explained in [3], when considering all the motors, the relation between the joint torques and their corresponding motor forces can be written as

$$\begin{bmatrix} \Gamma_h \\ \Gamma_k \\ \Gamma_a \end{bmatrix} = \begin{bmatrix} j_h & 0 & 0 & j_{h,hk} & 0 \\ 0 & j_k & 0 & j_{k,hk} & j_{k,ka} \\ 0 & 0 & j_a & 0 & j_{a,ka} \end{bmatrix} \cdot \begin{bmatrix} F_h \\ F_k \\ F_a \\ F_{hk} \\ F_{ka} \end{bmatrix}. \tag{3}$$

with Γ_h, Γ_k, and Γ_a being the hip, knee, and ankle joint torque, respectively, F_h, F_k, F_a, F_{hk}, and F_{ka} the forces provided by the actuators (see Figure 8).

In Eq. (2), the matrix containing all the $j_{\alpha,\beta}$ components will be referred simply as J. Something worth noting is that this 3×5 matrix which represents a three-joint/five-motor architecture will be modified when removing a motor by suppressing its corresponding column in the matrix. This highlights the nonredundant architectures limited to three motors (thus a 3×3 matrix) and the redundant ones with up to 5 actuators (thus 3×4 or 3×5 depending on the architecture).

As linear actuators are considered, generically, the real coefficient $j_{\alpha,\beta}$ is defined as the leverage between the actuator's axis $\overrightarrow{m_\beta}$ and the affected joint position P_α, defined as

$$j_{\alpha,\beta} = \frac{\left\| \overrightarrow{P_\alpha M_\beta} \times \overrightarrow{m_\beta} \right\|}{\left\| \overrightarrow{m_\beta} \right\|}, \tag{4}$$

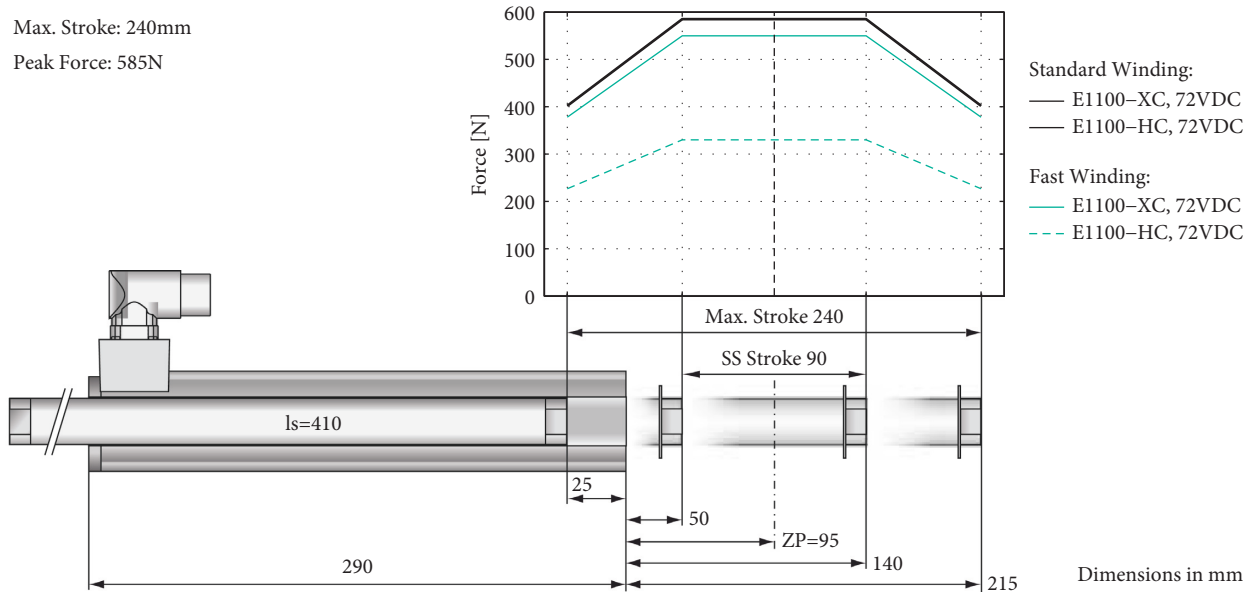

Figure 5: Standard DD electric linear motor characteristics (P01-48 × 240/30 × 240 from LinMot®).

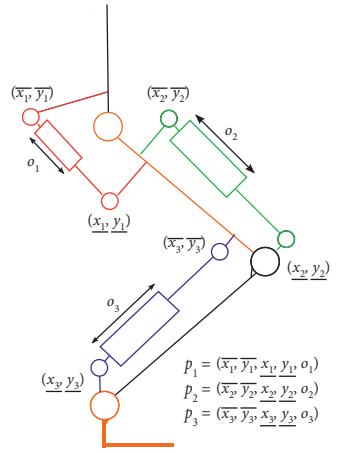

Figure 6: The geometry parameters for a given architecture.

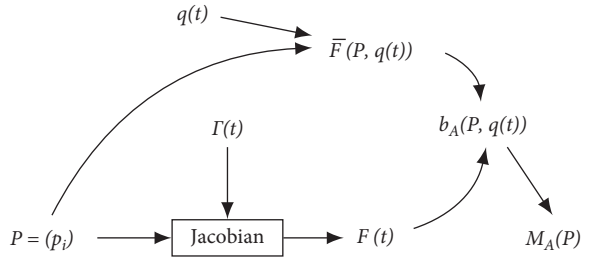

Figure 7: System inputs and outputs.

with M_β being a point belonging to the motor's line. In our case, the point M_β is chosen as a fixation point. Even though J is known, there might be some issues to be addressed depending on the architecture. In fact, for redundant architectures, there exist many admissible couples of forces. This situation is handled by performing an optimization of the motor's power. To do so, the motor's velocities are computed from the following:

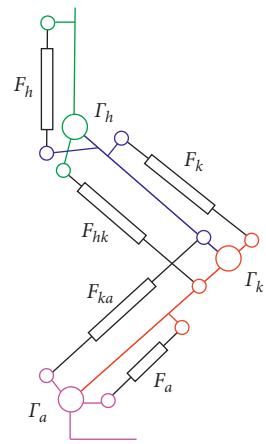

Figure 8: Actuator's forces and joint torques.

$$V_{\text{motors}} = J^T \cdot \frac{dq}{dt}, \tag{5}$$

with J^T the transpose of the matrix J linking the vector of torques Γ and the vector of forces F in (2). Then, an optimization is performed in order to find the forces distribution with minimal power while satisfying the torque requirement constraints. The latter optimization problem is defined as a least squares linear problem of the following form:

$$\min_F \left\{ \frac{1}{2} \left\| V_{\text{motors}} \cdot F \right\| \text{such that } \Gamma = J \cdot F \right\}. \tag{6}$$

If the required forces cannot be performed by the actuators, the optimization is redone without boundaries in order to still obtain a force distribution, even though the Boolean $b(p,t)$ will not be true.

The method to obtain the maximum available force of a motor $\overline{F}(p, q(t))$ is composed of two steps. First, the motor's elongation which corresponds to the distance between its two fixation points is computed. Then, the maximum force available for this length is retrieved from its datasheet (see Figure 5).

4. Numerical Optimization

The previously shown simulator is used within an optimization loop in order to obtain for each studied architecture an optimal placement of the motors. This optimization was implemented in the MATLAB® environment with the fminsearchbnd function, which uses the Nelder-Mead simplex method with boundaries to find a local minimum for a nonlinear problem. The following parts will present the practical choices made within the team to perform this optimization and the results are obtained.

4.1. Experimental Setup. To realize a numerical optimization, some concerns such as the robot's dimension and the studied motions must be addressed. In [7, 15], these elements were included as optimization variables instead of using preexisting or simulated data. For the sake of simplicity, and as the choice of the motor's type and number as well as their naive placement comes from mimicking the human leg structure, the robot's parameters and motions were chosen to be identical to those of a human subject. To do so, the geometric parameters and joint trajectories were picked from the HuMoD database [14]. We obtained them from a subject (A in the database) performing multiple motions on an instrumented treadmill while recorded by a motion capture system. This study focuses on squats, walking, and running motions available in the database. These motions are considered to be performed alone and consecutively. This leads to motion-specialized geometries as well as generic geometries for each architecture and evaluates their overall efficiency. A preemptive study was performed to check for motions considered impossible regarding the torques required and future bounds of the optimization algorithm.

Indeed, the selected motors can produce a force up to 585 N (P01-48 × 240/30 × 240 from LinMot®), so some available motions could be too demanding for the motors and should not be considered. This resulted in selecting the following motions:

Squats

Walking at 1, 1.5 and 2 m/s

Running at 2 m/s

Figures 9–11 show the joint torques required for a 3 m/s running as an example, which is not a part of the set of studied motions due to the motion being too demanding. Different leverages (from 5 to 20 centimeters) were then assumed with the maximum motor force available (585 N), and their corresponding torques were computed to draw feasible zones depending on the maximum leverage allowed. For instance, the knee joint would require 20 centimeters of leverage to generate the required torque. From this, faster running was considered too ambitious as it would require a leverage of at least 20 centimeters in order to perform with the selected motors.

Concerning the bounds for each motor's position (i.e., their fixation points), they are limited to a rectangle spanning the length of the limb attached to and up to 85 millimeters from the limb's axis. Last but not least, it is assumed that the

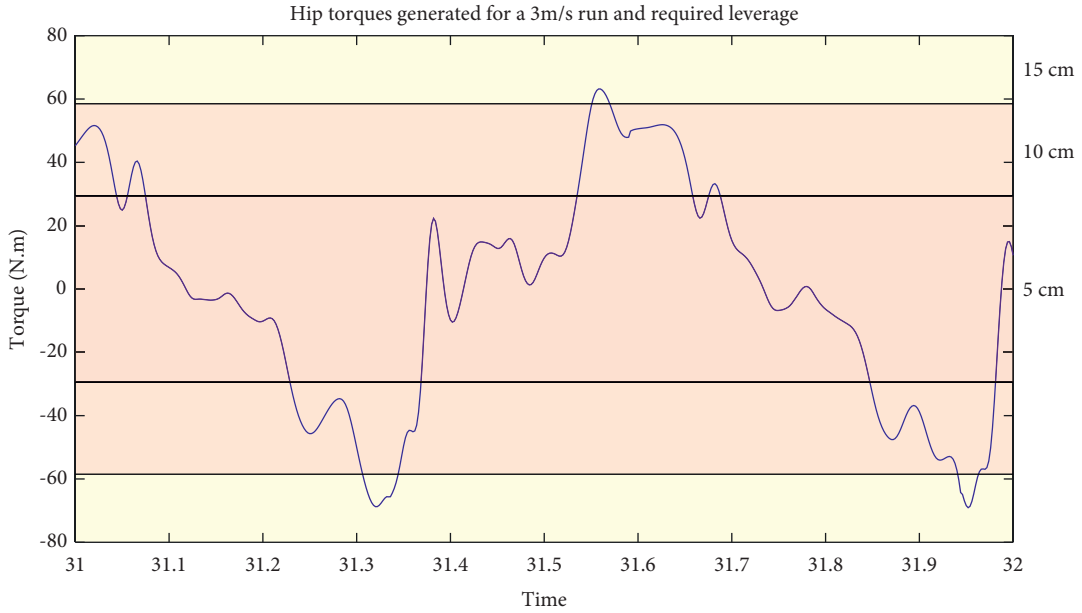

Figure 9: Hip torques for a 3 m/s run and leverage required.

robot will have masses and inertia matrices identical to the HuMoD subsect. With all these assumptions in mind, a cluster was put up to perform multiple optimizations in parallel. This allows us to optimize all the considered architectures simultaneously for a given set of motions. An experiment (i.e., an optimization of all the architectures for one set of motions) takes up to one week, as for each instant (30,000 to 50,000 time-stamped instants per motion) the actuator's positions, maximal and required forces are computed. An evaluation takes up to 5 minutes to be performed in the case that all the motions are taken into account.

For the following results, a threshold of 95% was fixed to consider a motion feasible by a given architecture. The convergence time and feasibility values were recorded during the optimization process and are shown in Figure 12. Furthermore, the motor forces, once the optimal geometries were obtained, were computed (see Figures 13–17). The source code for the simulator is available online at https://laris.univ-angers.fr/fr/projets/projets-actuels/robibio.html. The following sections will present our results when considering a single motion or multiple motions at once.

4.2. Specialized Geometries. This section concerns the optimization results obtained when considering each motion separately. Each value shown in Figure 18 represents the best feasibility obtained by an architecture for a given motion. A noticeable gap can be seen between the nonredundant and redundant architectures. In fact, only redundant architectures can perform up to the running motion, with architecture 11 being an exception as only one motor is actuating the knee joint. Moreover, there is only one architecture with an existing geometry to perform each motion entirely, namely, the five-motor architecture number 14. However, the four-motor architecture number 12 can still pass the threshold for every studied motion. The nonredundant architecture cannot perform beyond walking at 1 m/s. In this aspect, architecture 8 (Figure 19) can be highlighted as the only three-motor architectures with geometries able to perform the squat or the walking motion. It is worth noting that, for the squat motion, it is mandatory to have two motors affecting the hip joint (the monoarticular hip and the bi-articular hip-knee), hence the need of bi-articular actuators.

4.3. Versatile Geometries. With multiple motions, the first experiment takes two of them simultaneously: the squat and the walking motion at 1 m/s. We then add one motion after the other for each new experiment until all five motions are considered. In practice, the additional motions are added to the joint trajectory vectors. Here, only redundant architectures seem to have the potential to perform multiple motions, as shown in Figure 20. As in the previous case, only architecture 14 (i.e., the 5-actuator architecture) has a solution satisfying all the motion requirements. It can be noted that when disregarding the running motion, architectures 12 (Figure 21) and 13 are valid alternatives even though they use only 4 actuators.

4.4. Discussion. In this paper, all the optimizations are performed considering the complete timeline of the HuMoD motions. Indeed, we could have restricted our attention to a cycle considered representative of the whole trajectory. However, it led to specialized optimal solutions for the given "representative" cycle. From the previously shown results, electric DD linear motors appear as a valid actuation scheme when operating a biped robot. A bi-articular motor and a larger scale redundancy can greatly improve the capabilities of a biped robot compared to a classic 3 joints/3

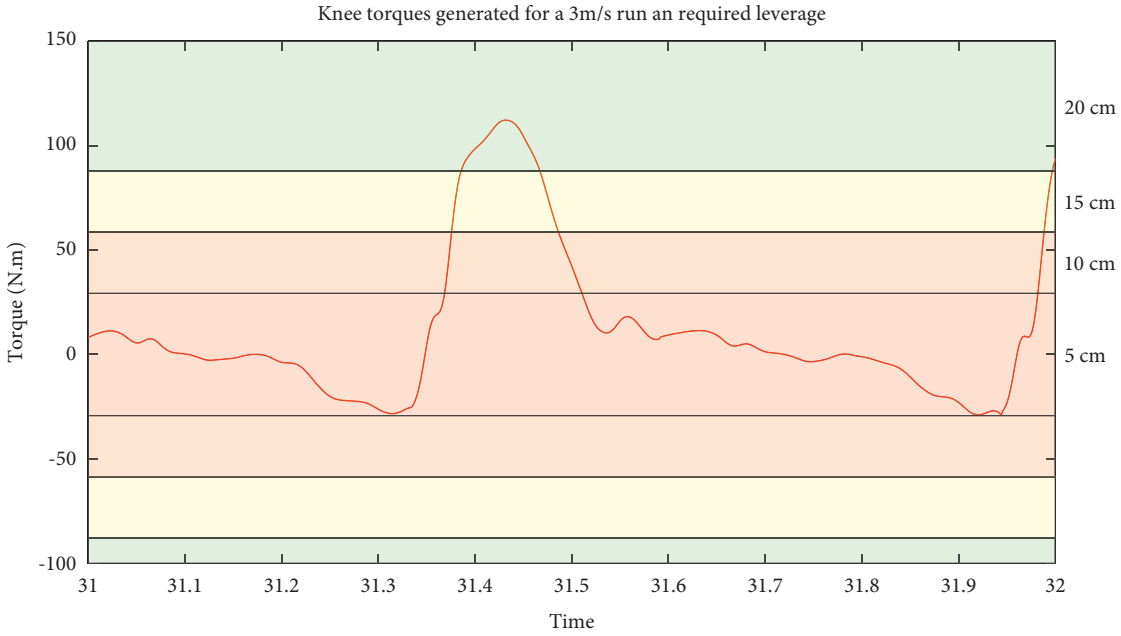

Figure 10: Knee torques for a 3 m/s run and leverage required.

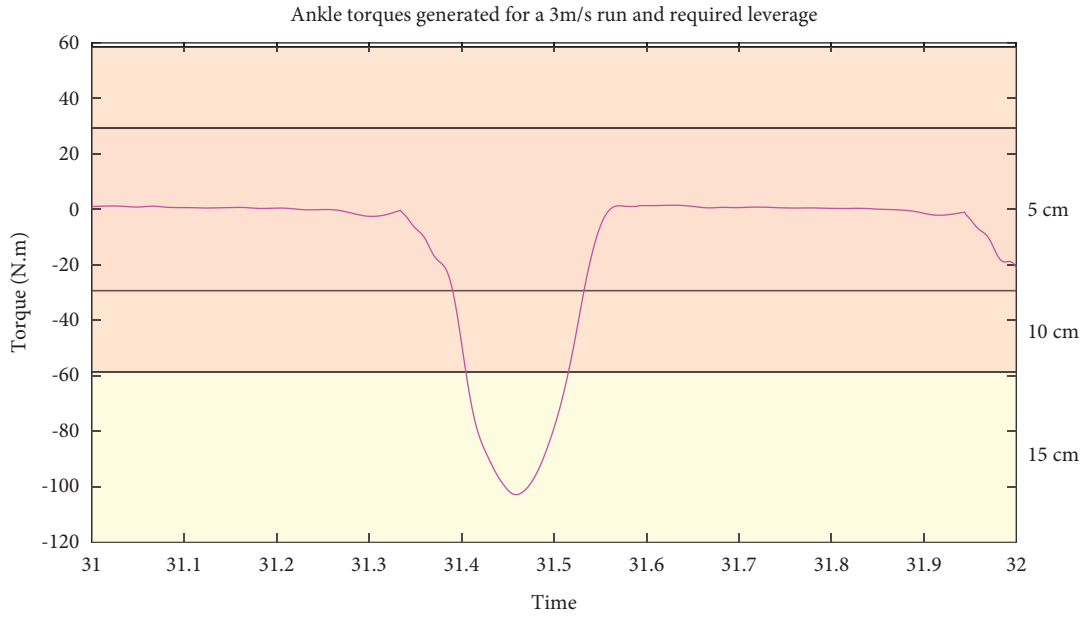

Figure 11: Ankle torques for a 3 m/s run and leverage required.

monoarticular actuator architecture. The optimality of the results is an issue as our system possesses a high number of local minima. Furthermore, even though architecture 14 is able to perform nearly 100% of the studied motions, Figure 22, which exposes the optimal geometry for each architecture, shows that possible collisions between the actuators and/or body segments might be an issue that should be addressed.

Future work involves the validation of the architectures with real actuator masses in a 3D modeling software as well as performing a new set of optimizations with more powerful actuators. Finally, we expect to start building a robot with such actuation in the upcoming months to verify these theoretical results. This work could also be reproduced with input torques obtained from an optimized joint trajectory for a specific motion to confirm these results.

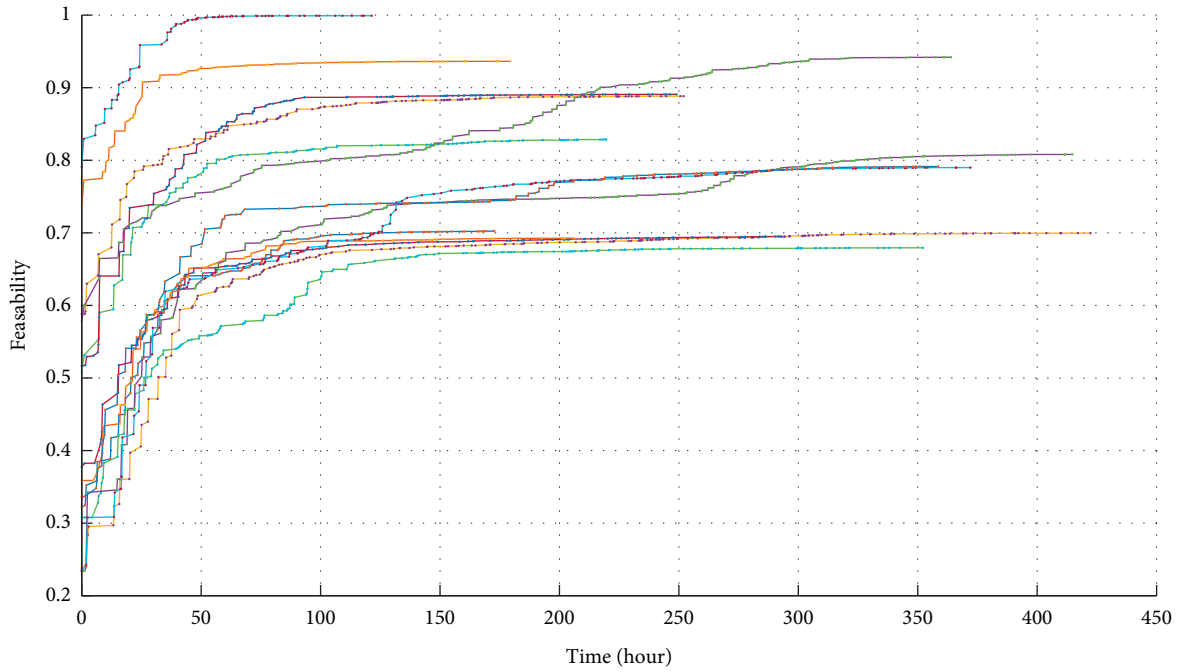

Figure 12: Convergence time of the optimization process.

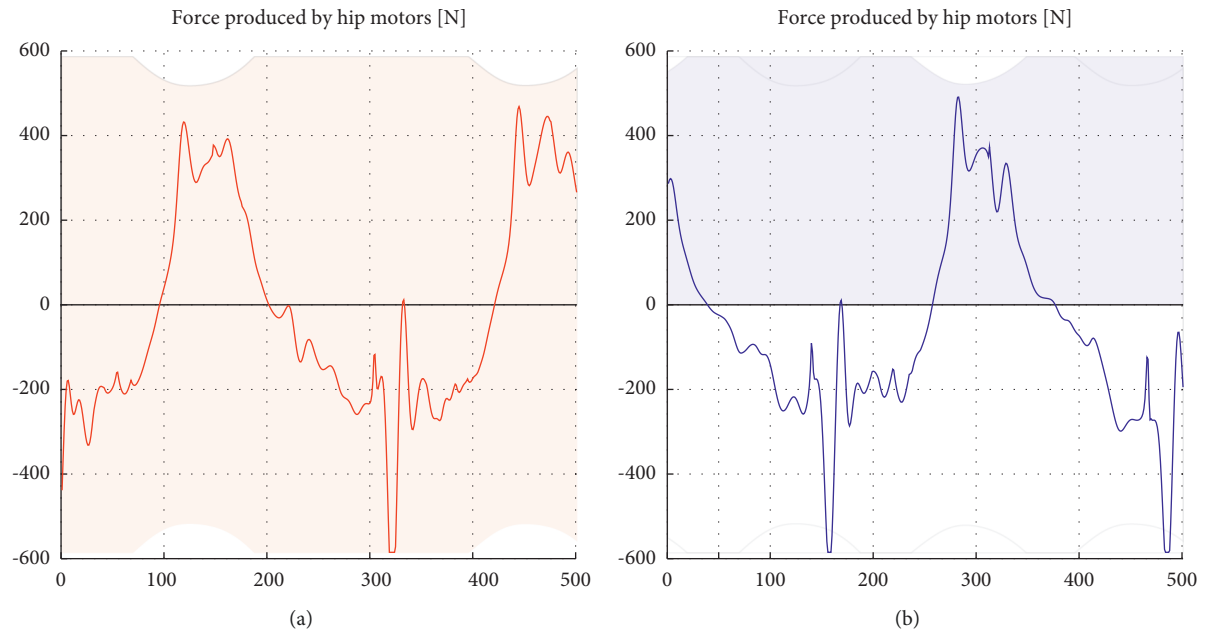

Figure 13: Kip motor force for the optimal geometry of architecture 14 (red: (a), blue: (b)).

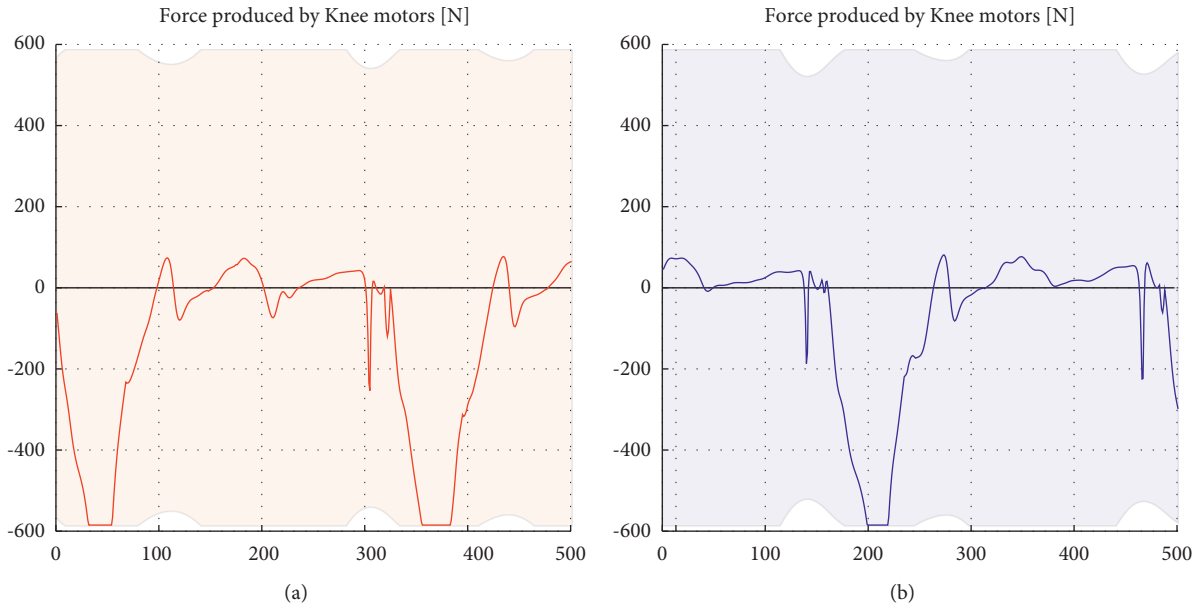

Figure 14: Knee motor force for the optimal geometry of architecture 14 (red: (a), blue: (b)).

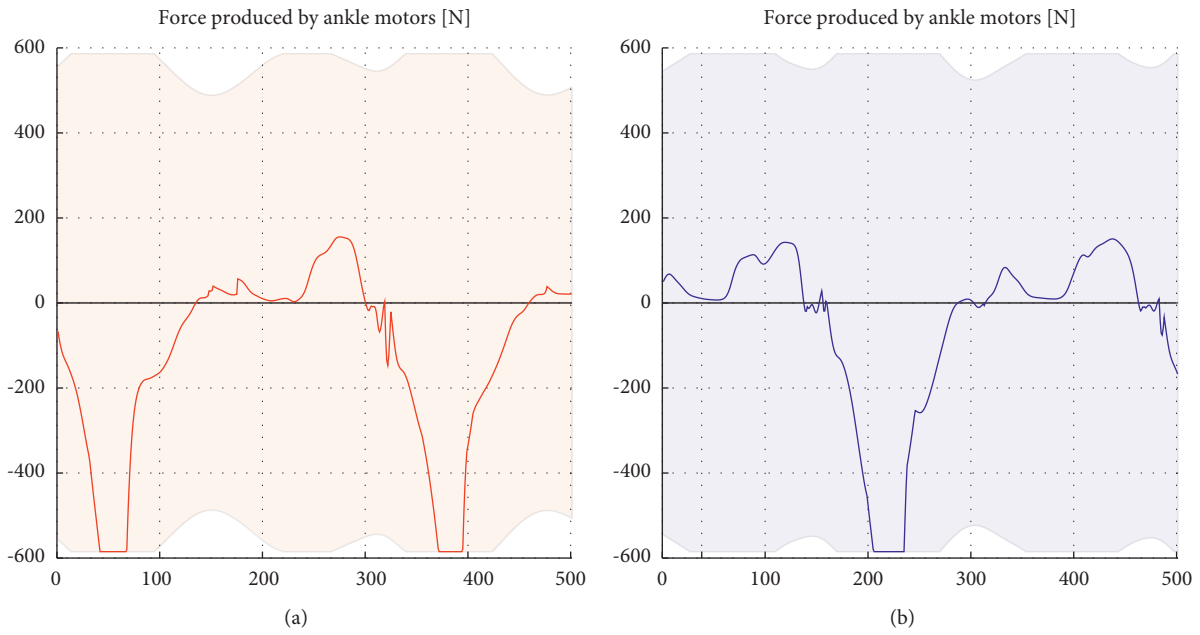

Figure 15: Ankle motor force for the optimal geometry of architecture 14 (red: (a), blue: (b)).

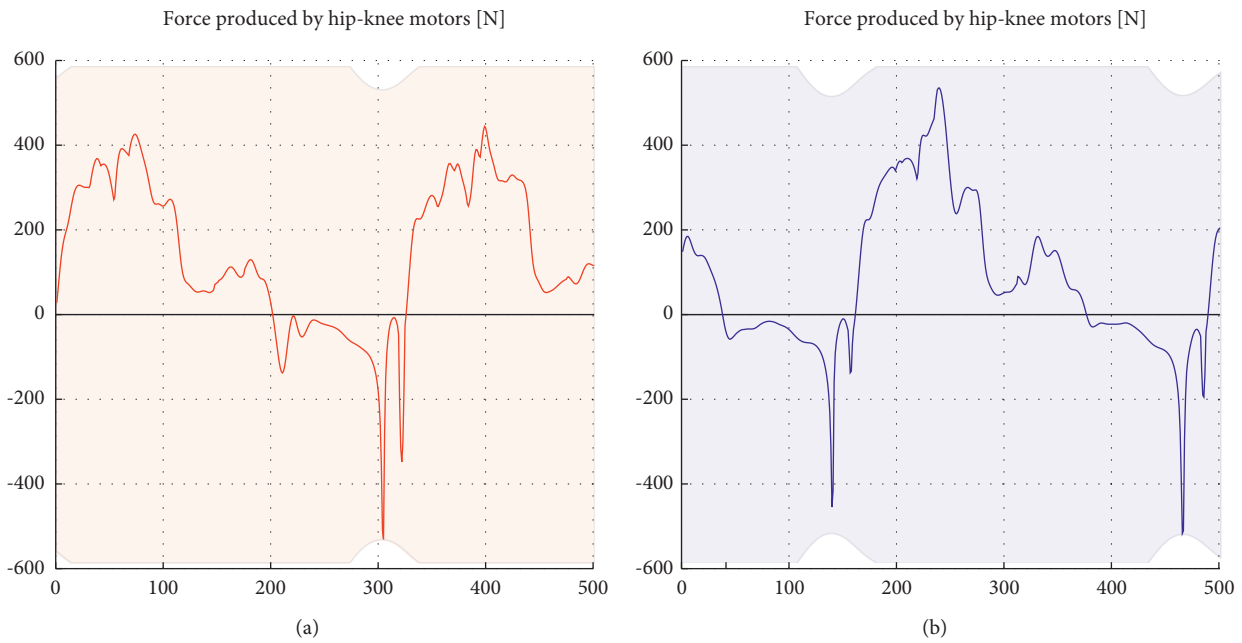

Figure 16: Hip-knee motor force for the optimal geometry of architecture 14 (red: (a), blue: (b)).

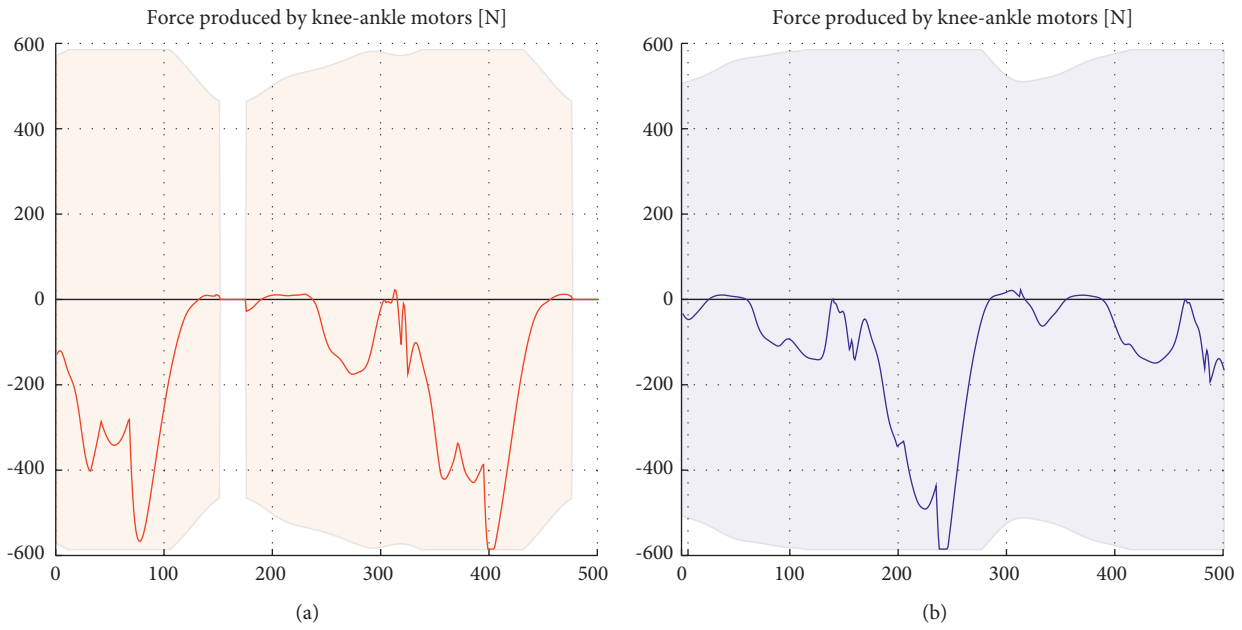

Figure 17: Knee-ankle motor force for the optimal geometry of architecture 14 (red: (a), blue: (b)).

	Hip	Knee	Ankle	Hip-knee	Knee-ankle	Architecture	Squat	Walking 1m/s	Walking 1.5m/s	Walking 2m/s	Running 2m/s
3 motors	■	■	■			1	73, 74%	82, 23%	72, 16%	72, 65%	59, 41%
		■	■	■		2	68, 23%	75, 02%	62, 62%	50, 59%	60, 08%
	■		■		■	3	87, 47%	80, 44%	66, 98%	66, 95%	66.88%
	■		■	■		4	95, 35%	81, 10%	68, 74%	70, 82%	60.36%
			■	■	■	5	76, 20%	97, 96%	86, 15%	68, 66%	64.94%
	■	■			■	6	90, 29%	98, 25%	84, 30%	84, 55%	81.83%
		■		■	■	7	76, 07%	99, 10%	85, 34%	80, 39%	82.70%
	■			■	■	8	98, 29%	97, 57%	82, 30%	82, 87%	85.33%
4 motors	■	■	■		■	9	92, 66%	99, 92%	99, 79%	96, 99%	96.63%
	■	■	■	■		10	100, 00%	82, 60%	84, 27%	87, 17%	68, 04%
		■	■	■	■	11	90, 46%	99, 85%	99, 79%	96, 85%	96, 77%
	■		■	■	■	12	100, 00%	100, 00%	99, 92%	98, 94%	100, 00%
	■	■		■	■	13	100, 00%	99, 58%	98, 41%	87, 41%	86, 64%
5 motors	■	■	■	■	■	14	100, 00%	100, 00%	99, 90%	99, 90%	100, 00%

Figure 18: Feasibilities after optimization for each motion.

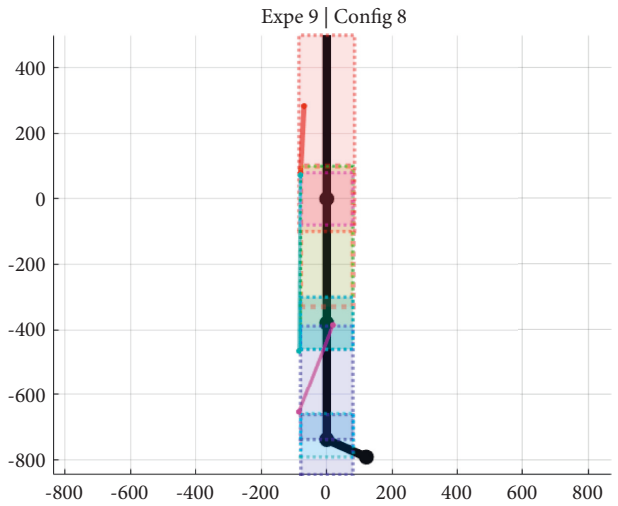

Figure 19: Optimal specialized geometry for architecture 8.

	Hip	Knee	Ankle	Hip-knee	Knee-ankle	Architecture	Squat	Squat	Squat	Squat
							Walking 1m/s	Walking 1 m/s	Walking 1 m/s	Walking 1 m/s
								Walking 1,5 m/s	Walking 1,5 m/s	Walking 1,5 m/s
									Walking 2 m/s	Walking 2 m/s
										Running 2 m/s
3 motors	■	■	■			1	76,38%	74.04 %	73.30 %	70.26 %
		■	■	■		2	77,90%	74.66 %	72.71 %	69.97 %
	■		■		■	3	74,47%	70.46 %	68.68 %	67.94 %
	■		■	■		4	82,27%	73.42 %	71.42 %	69.51 %
			■	■	■	5	87,92%	84.07 %	77.92 %	69.26 %
	■	■			■	6	86,16%	80.43 %	80.18 %	80.81 %
		■		■	■	7	87,94%	84.50 %	79.23 %	78.99 %
	■			■	■	8	91,51%	84.80 %	79.49 %	79.14 %
4 motors						9	89,91%	92.93 %	93.14 %	88.83 %
						10	89,17%	86.57 %	87.03 %	82.88 %
						11	95,21%	95.79 %	92.05 %	89.08 %
						12	100,00%	99.94 %	99.39 %	93.63 %
						13	99,77%	98.15 %	97.02 %	94.13%
5 motors						14	100,00%	99.96 %	99.92 %	99.92 %

Figure 20: Feasibilities after optimization for cumulative motions.

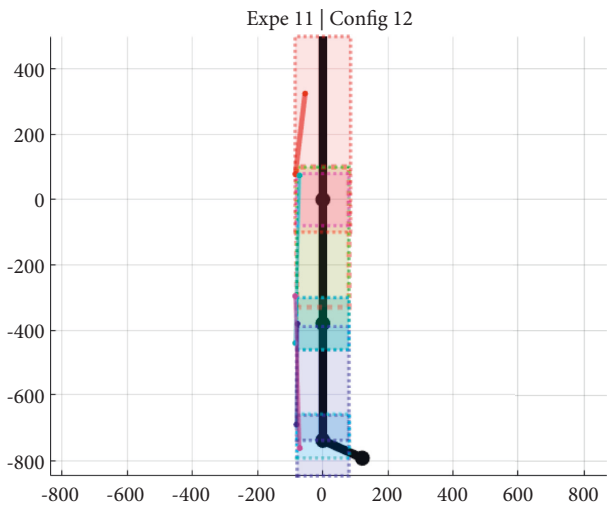

Figure 21: Optimal versatile geometry for architecture 12.

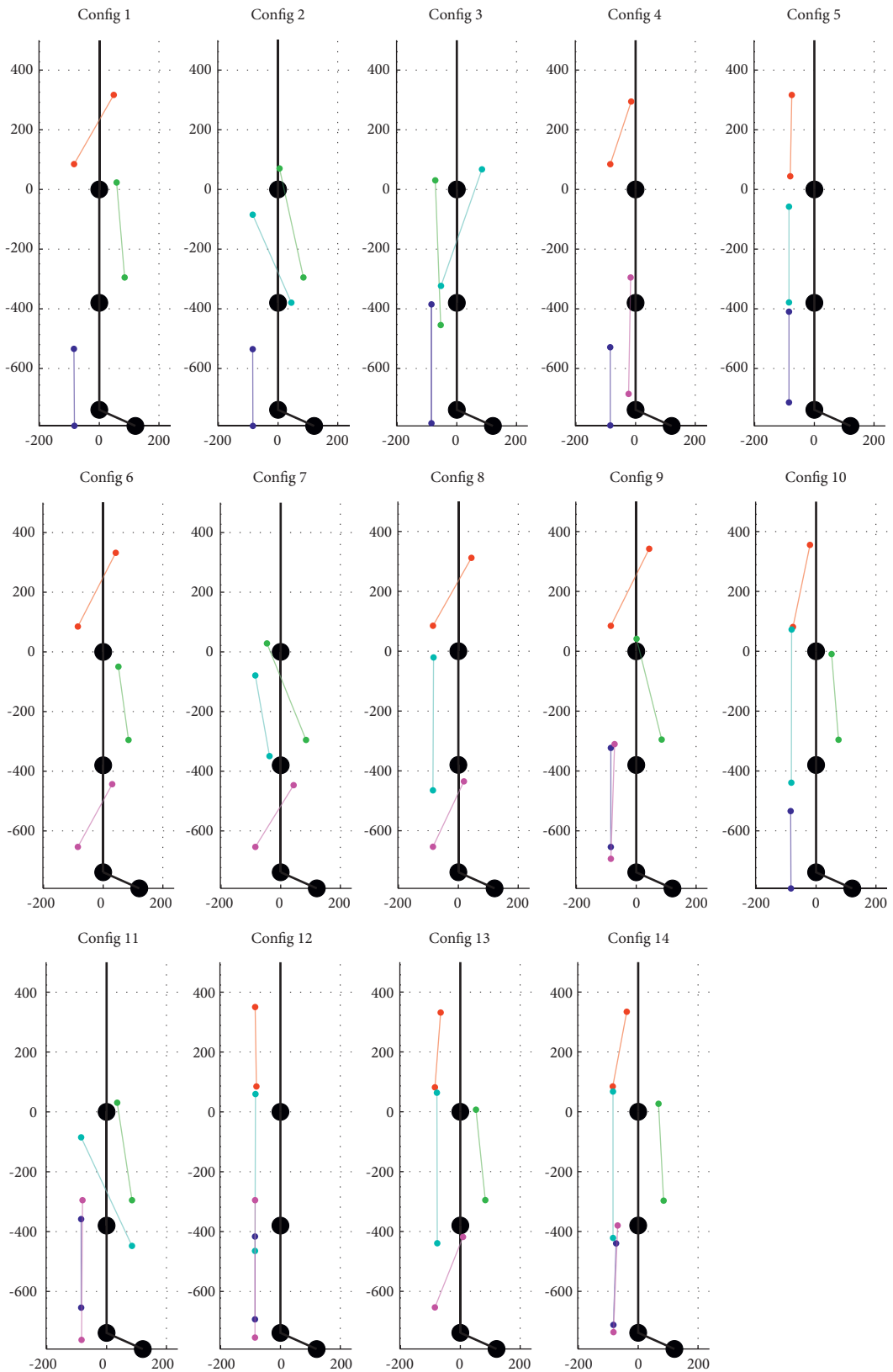

Figure 22: Optimal geometries for each architecture.

Table 1: HuMoD parameters.

Segment	Length (m)	Mass (kg)
Head	0.275	3.838
Upper arm	0.248	1.282
Lower arm	0.245	1.061
Thorax	0.228	15.067
Pelvis	Along Y: 0.124 Along *Z*: 0.187	8.364
Thigh	0.380	8.332
Shank	0.358	2.573
Foot	Along *X*: 0.121 Along Y: 0.054 Along *Z*: 0.034	0.570

5. Conclusion and Perspectives

This study investigates the potential of electric DD linear motors for the actuation scheme of a planar biped robot. We also considered the use of bi-articular motors and redundant architectures. Such motors are an interesting alternative to rotative actuators and allow more freedom in their positioning. Furthermore, relying on bi-articular actuators can increase the available torque on a specific joint to perform a motion that would be impossible with only monoarticular actuators. Redundancy seems like a prerequisite in order to perform high-dynamic motions such as fast walking and running. Many development choices were made, such as the actuators chosen (new models seem to be able to deliver over 1000 N), their number and position, as well as the hypothesis concerning the actuator masses. (Table 1).

Data Availability

The source code of the simulator is available online at https://laris.univ-angers.fr/fr/projets/projets-actuels/robibio.html.

Conflicts of Interest

The authors declare that they have no conflicts of interest.

References

[1] M. Raibert, *Legged Robots that Balance*, MIT Press, Cambridge, MA, USA, 1986.

[2] H. Kaminaga, J. Ono, Y. Nakashima, and Y. Nakamura, "Development of Backdrivable Hydraulic Joint Mechanism for Knee Joint of Humanoid Robots," in *Proceedings of the 2009 IEEE International Conference on Robotics and Automation*, pp. 1577–1582, Kobe, Japan, May 2009.

[3] C. Chevallereau, P. Wenger, Y. Aoustin, F. Mercier, N. Delanoue, and P. Lucidarme, "Leg design for biped locomotion with mono-articular and bi-articular linear actuation," *Mechanism and Machine Theory*, vol. 156, Article ID 104138, 2021.

[4] Z. Li, S. Bai, O. Madsen, W. Chen, and J. Zhang, "Design, modeling and testing of a compact variable stiffness mechanism for exoskeletons," *Mechanism and Machine Theory*, vol. 151, Article ID 103905, 2020.

[5] M. Raibert, K. Blankespoor, G. Nelson, and R. Playter, "BigDog, the rough-terrain quadruped robot," *IFAC Proceedings Volumes*, vol. 41, no. 2, pp. 10822–10825, 2008.

[6] A. Rosendo, S. Nakatsu, K. Narioka, and K. Hosoda, "Pneupard: a biomimetic musculoskeletal approach for a feline-inspired quadruped robot," in *Proceedings of the 2013 IEEE/RSJ International Conference on Intelligent Robots and Systems*, pp. 1452–1457, Tokyo, Japan, November 2013.

[7] A. Spielberg, B. Araki, C. Sung, R. Tedrake, and D. Rus, "Functional co-optimization of articulated robots," in *Proceedings of the 2017 IEEE International Conference on Robotics and Automation (ICRA)*, pp. 5035–5042, Singapore, May 2017.

[8] P. M. Wensing, A. Wang, S. Seok, D. Otten, J. Lang, and S. Kim, "Proprioceptive actuator design in the MIT cheetah: impact mitigation and high-bandwidth physical interaction for dynamic legged robots," *IEEE Transactions on Robotics*, vol. 33, no. 3, pp. 509–522, 2017.

[9] K. Hirai, M. Hirose, Y. Haikawa, and T. Takenaka, "The development of Honda humanoid robot," in *Proceedings of the 1998 IEEE International Conference on Robotics and Automation (Cat. No.98CH36146)*, vol. 2, pp. 1321–1326, Leuven, Belgium, May 1998.

[10] M. A. Sharbafi, C. Rode, S. Kurowski et al., "A new biarticular actuator design facilitates control of leg function in BioBiped3," *Bioinspiration I& biomimetics*, vol. 11, no. 4, Article ID 046003, 2016.

[11] S. Kalouche, "GOAT: a legged robot with 3D agility and virtual com4pliance," in *Proceedings of the 2017 IEEE/RSJ International Conference on Intelligent Robots and Systems (IROS)*, pp. 4110–4117, Vancouver, BC, Canada, September 2017.

[12] P. Jakubik, "An autonomous biped: concept and design," in *ICINCO 2012 - Proceedings of the 9th International Conference on Informatics in Control, Automation and Robotics*, vol. 2, pp. 167–176, Rome, Italy, January 2012.

[13] C. A. M. Doorenbosch, G. J. van Ingen Schenau, and Gerrit Jan van Ingen Schenau, "The role of mono- and bi-articular muscles during contact control leg tasks in man," *Human Movement Science*, vol. 14, no. 3, pp. 279–300, 1995.

[14] J. Wojtusch and O. von Stryk, "HuMoD - a versatile and open database for the investigation, modeling and simulation of human motion dynamics on actuation level," in *Proceedings of the 2015 IEEE-RAS 15th International Conference on Humanoid Robots (Humanoids)*, pp. 74–79, Seoul, Korea (South), November 2015.

[15] S. Ha, S. Coros, A. Alspach, J. Kim, and K. Yamane, "Computational co-optimization of design parameters and motion trajectories for robotic systems," *The International Journal of Robotics Research*, vol. 37, no. 13-14, pp. 1521–1536, 2018.